Journal of Hazardous Materials 182 (2010) 570–580

Contents lists available at ScienceDirect

Journal of Hazardous Materials

journal homepage: www.elsevier.com/locate/jhazmat

A comparison of gray and non-gray modeling approaches to radiative transfer in pool fire simulations

Gautham Krishnamoorthy*

Department of Chemical Engineering, PO Box 7101, Harrington Hall Room 323, 241 Centennial Drive, University of North Dakota, Grand Forks, ND 58202-7101, USA

ARTICLE INFO

Article history:
Received 17 March 2010
Received in revised form 10 May 2010
Accepted 17 June 2010
Available online 23 June 2010

Keywords:
Radiation modeling
Pool fires
Discrete ordinates
Radiation blockage
Non-gray models

ABSTRACT

Decoupled radiative heat transfer calculations of 30 cm-diameter toluene and heptane pool fires are performed employing the discrete ordinates method. The composition and temperature fields within the fires are created from detailed experimental measurements of soot volume fractions based on absorption and emission, temperature statistics and correlations found in the literature. The measured temperature variance data is utilized to compute the temperature self-correlation term for modeling turbulence–radiation interactions. In the toluene pool fire, the presence of cold soot near the fuel surface is found to suppress the average radiation feedback to the pool surface by 27%. The performances of four gray and three non-gray radiative property models for the gases are also compared. The average variations in radiative transfer predictions due to differences in the spectroscopic and experimental databases employed in the property model formulations are found to be between 10% and 20%. Clear differences between the gray and non-gray modeling strategies are seen when the mean beam length is computed based on traditionally employed geometric relations. Therefore, a correction to the mean beam length is proposed to improve the agreement between gray and non-gray modeling in simulations of open pool fires.

1. Introduction

Numerical simulations of hydrocarbon pool fires can provide valuable insights into fire prevention, safety and extinction. Radiation is an important mode of heat transfer in pool fires. The fire hazard of a fuel is characterized to an important extent by the total radiative output of a fire to its surroundings and the radiative fluxes and feedback to the pool surface can determine the rate of fuel pyrolysis and evaporation. To spatially and temporally resolve its important flow characteristics, transient simulations of the fire are usually performed on computational grids frequently exceeding 10^6 computational cells [1]. Since radiation is often solved on the same grid that is employed to resolve the flow, its calculation in these simulations can get quite expensive due to its angular and wavelength dependencies. The optimal angular resolutions to use in the radiation calculations in pool fire simulations have been discussed in previous studies by Jensen et al. [1] and Hostikka [2]. This study focuses on optimizing the spectral dependency of the radiation calculation. The soot in pool fires can often be modeled as a gray body. However, the fire modeler has a wide range of gray and non-gray gas radiative property models to choose from that vary in speed, accuracies and the spectroscopic databases that were employed in the model formulation. For instance, gray or total radiative properties of gas mixtures can be obtained in the form of total emissivities or total transmissivities from: (a) correlations that have been fit to experimental data [3]; (b) wide band models by first obtaining band absorptances and then integrating them over the spectrum to get a total property [4]; (c) narrow band models by first obtaining narrow band properties in $\sim$25 cm^{-1} wavenumber intervals and then integrating them over the spectrum to get the total property [5]. Emissivities and transmissivities are path length dependant properties that are computed at each computational cell in computational fluid dynamics (CFD) simulations by taking a suitable geometric mean beam length of the geometry as the path length. The geometric relations to compute the path length have been well established in systems such as boilers and furnaces where the entire domain is radiatively participating. However, in simulations of open pool fires the selection of a path length is not obvious since only a fraction of the domain is radiatively participating. For instance, in optically thick pool fires where the path length of radiation is small, Snegirev [6] employed the cell size as the mean beam length. Hostikka [2] computed the path length by multiplying the geometric mean beam length of the domain by the fraction of the domain that was occupied by the fire. To address these issues, decoupled radiative transfer calculations of a heptane and toluene pool fire are performed in this paper.

* Tel.: +1 701 777 6699; fax: +1 701 777 3773.
E-mail address: gautham.krishnamoorthy@und.edu.

0304-3894/$ – see front matter © 2010 Elsevier B.V. All rights reserved.
doi:10.1016/j.jhazmat.2010.06.071

1. Gas phase radiative properties are predicted employing four gray and three non-gray models to examine the variations in the radiative transfer predictions due to gray and non-gray modeling strategies as well as due to differences in the spectroscopic and experimental databases employed in the property model formulations.
2. By comparing the radiative fluxes obtained from the gray models against path length independent non-gray model calculations, a correction to the mean beam length is proposed to improve the agreement between the gray and non-gray models.

The decoupled calculations are performed on fixed temperature and specie fields that are representative of conditions within the fire. These can either be obtained from CFD simulations of the fire and then freezing the flow [1] or through interpolations and extrapolations of detailed experimental data [7,8]. The latter approach has been adopted in this study due to the following reasons:

1. It establishes a validation methodology to directly compare model outputs against experimental measurements without the inherent errors and uncertainties associated with the turbulence and combustion models in a CFD calculation.
2. Predicting soot concentrations accurately in numerical simulations of turbulent diffusion flames remains a challenge due to the complex chemical mechanisms and long time scales governing soot formation. Since pool fires can vary widely in size and sooting propensities, employing detailed experimental measurements of soot concentrations to create the conditions within the fire will enable a study of a wide range of fires.
3. Carefully selecting experimental datasets that report soot volume fractions based on absorption as well as emission, enables one to examine the suppression of the radiation feedback to the pool surface due to the presence of cold soot near the fuel surface. This can strongly influence the rate of fuel pyrolysis and evaporation.

The pool fires examined in this study are described next.

2. Description of cases

Synthetic fire fields were created from experimental data obtained from a 30 cm diameter toluene and a 30 cm diameter heptane pool fire by Klassen and Gore [9]. Radial profiles of the mean and standard deviation of temperature and soot volume fractions at seven axial locations were reported in an easily accessible tabular form making it an ideal dataset for use in this study. After assuming that the optical constants of soot were described by the data of Dalzell and Sarofim [10], Klassen and Gore [9] inferred the soot volume fractions based on absorption (cold soot) and emission (hot soot) from absorption and two-wavelength emission measurements. The flame heights of both the fires were estimated to be 1.3 m. In this paper, we employ the experimental data of Klassen and Gore [9] in conjunction with the correlations from the literature to describe the spatial variations in mean temperature, standard deviation of temperature and mean soot concentrations within the fire [11,12]. First, the centerline variation of these variables was determined by fitting the centerline experimental data with cubic splines. The radial profiles were then fit to the experimental data by assuming a Gaussian variation. If z is the axial distance and Q the total heat release in the fire (125 kW for the toluene fire and 116 kW for the heptanes fire), then z' is defined as:

$$z' = \frac{z}{Q^{0.4}} \tag{1}$$

McCaffrey [11] identified 3 zones in a pool fire, laminar ($z' < 0.04$), intermittent ($0.04 < z' < 0.08$) and buoyant ($z' > 0.08$). In the lower part of the flame ($z' < 0.04$), if ΔT_{CL} is the mean axial temperature rise from the ambient (298 K) then ΔT the corresponding mean radial temperature rise was fit to the form [10]:

$$\frac{\Delta T}{\Delta T_{CL}} = \exp\left[\left(\frac{x_m}{\sigma_1}\right)^2\right] \exp\left[-\left(\frac{x - x_m}{\sigma_2}\right)^2\right] \quad \text{for } x \geq x_m \tag{2}$$

$$\frac{\Delta T}{\Delta T_{CL}} = \exp\left[\left(\frac{x_m}{\sigma_1}\right)^2\right] \quad \text{for } x < x_m$$

where

$$x = \frac{r}{R}$$

$$x_m = \exp\left[(0.9Q - 205)z'\right]$$

$$\sigma_1 = 0.4 + x_m$$

$$\sigma_2 = 0.5 - 0.4x_m$$

Here, R is the radius of the pool fire and r is the radial distance from the pool center. In the intermittent and buoyant regions:

$$\frac{\Delta T}{\Delta T_{CL}} = \exp\left[\left(\frac{x_m}{\sigma_3}\right)^2\right] \tag{3}$$

$$\sigma_3 = C_1 Q^{0.4}$$

C_1 was adjusted to vary linearly from 0.01 to 0.015 in the intermittent region and was set equal to 0.015 in the buoyant region. The mean temperature profiles at various axial and radial locations in the toluene pool fire are shown in Fig. 1. Fig. 2 shows the axial and radial mean temperature profiles in the 30 cm heptane pool fire. The radial variations in the standard deviation of temperature were fit to the equation [12]:

$$\frac{\sqrt{T'^2}}{T_{CL}} = C_2 \exp\left[-\left(\frac{x/z}{C_3}\right)^2\right] \tag{4}$$

C_2 was made to vary from 0.3 to 1.5 and C_3 varies from 0.1 to 5 across the various zones. The radial variations in emission and absorption soot volume fractions (fv_{soot}) were also fit to the form of a Gaussian distribution:

$$\frac{fv_{soot}}{fv_{soot,CL}} = \exp\left[-\left(\frac{r}{\sigma_4}\right)^2\right] \tag{5}$$

$$\sigma_4 = C_4 Q^{0.4}$$

In Eq. (5), C_4 was set to 0.014 and $fv_{soot,CL}$ represents the centerline soot volume fractions.

Fig. 3 shows the radial profiles of the mean emission and absorption soot volume fraction at various axial locations in the toluene pool fire. Fig. 4 shows the corresponding radial profiles for the mean emission and absorption soot volume fractions at different axial locations in the heptane pool fire. Klassen and Gore [9] reported that the measured absorption soot volume fractions were a true measure of volume fraction of soot whereas the emission soot volume fractions were a measure of relatively hot soot particles. Therefore, in this study, the difference between the absorption and emission soot volume fractions represented the volume fractions of "cold soot" particles whose temperatures were set at 298 K.

The decoupled radiation calculations in this study were performed on a 3D domain. 3D fields of the 2D experimental dataset were generated assuming axial symmetry. The temperatures of the computational cells that did not represent the fire were set at 298 K.

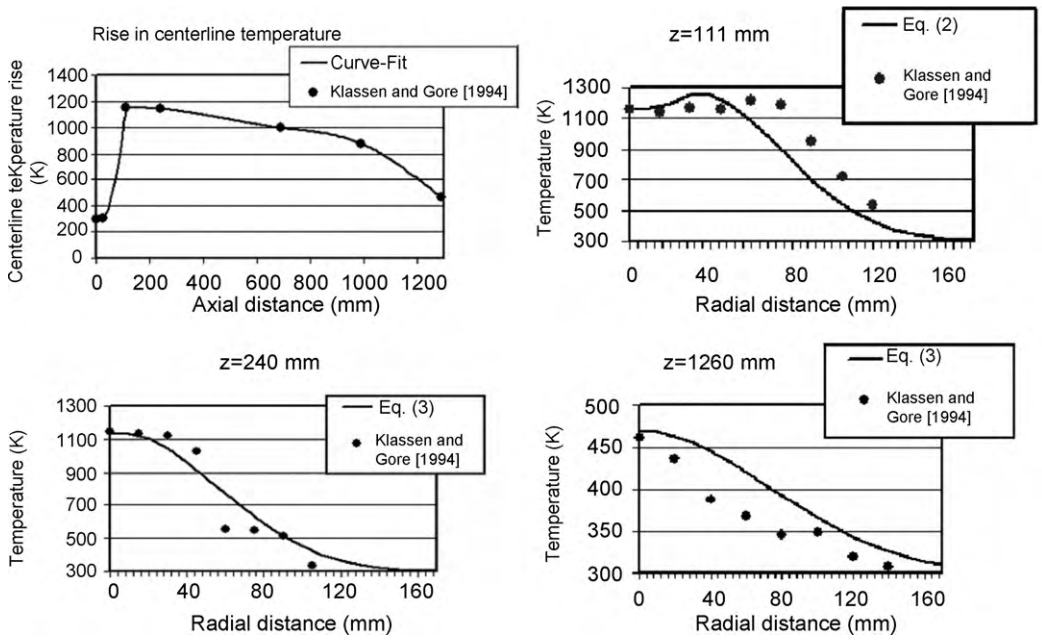

Fig. 1. The mean temperature profiles at various axial and radial locations in the 30 cm toluene pool fire.

The domain boundaries were assumed to be black and at a temperature of 298 K. The CO_2 and H_2O mole fractions (X) were estimated from the temperature measurements according to the equation [13]:

$$\text{average mole fraction} = (\text{stoichiometric mole fraction}) \times \left(\frac{\text{local flame temperature} - \text{ambient temperature}}{\text{adiabatic flame temperature for a stoichiometric mixture} - \text{ambient temperature}}\right)$$

For toluene:

$$X_{CO_2} = \left(\frac{7}{45}\right)\left(\frac{T-298}{T_{ad}-298}\right)$$

$$X_{H_2O} = \left(\frac{4}{45}\right)\left(\frac{T-298}{T_{ad}-298}\right) \quad (6)$$

For heptane:

$$X_{CO_2} = \left(\frac{7}{56}\right)\left(\frac{T-298}{T_{ad}-298}\right)$$

$$X_{H_2O} = \left(\frac{8}{56}\right)\left(\frac{T-298}{T_{ad}-298}\right) \quad (7)$$

T_{ad} is the adiabatic flame temperature (2274 K for heptane and 2338 K for toluene). It should be pointed out that the purpose of this study is not a comprehensive validation but to obtain insights into the performances of various gas radiative property models in these fires. In lieu of this objective, the observed agreement in Figs. 1–4 between the experimental measurements and the correlations may be deemed as acceptable. The radiative property models employed in this study are described next.

3. Gas radiative property models

The gray gas absorption coefficient (k) was computed from the total emissivities (ε) and path length (L) as:

$$k = -\frac{1}{L}\ln(1-\varepsilon) \quad (8)$$

Since the volume of the radiatively participating medium was roughly one-tenth the volume of the domain, the path length was computed by correcting the geometric mean-beam length by 0.1 as:

$$L = 0.1\frac{3.6V}{A} \quad (9)$$

In Eq. (9), V is the volume of the domain and A the total surface area.

3.1. Smith weighted-sum-of-gray-gases model (WSGGM) [14]

Since the H_2O/CO_2 ratios of the two fires considered in this study are 0.57 and 1.14 respectively, the Smith WSGG model [14] coefficients corresponding to a H_2O/CO_2 ratio of 1 was employed to estimate the gas emissivities. This model was employed in a gray as well as non-gray fashion. In the gray version, the temperature independent absorption coefficients and temperature dependant weighting fractions were employed to compute total emissivities of gas mixtures from which gray gas absorption coefficients were computed at each cell using Eq. (8). The results from this model are designated as "Smith" in this study. The non-gray version of model employs four gray gases (4 GG) to model the spectral dependencies and the results from the model are designated as "Smith (4 GG)."

3.2. Perry's handbook correlations

In the 8th edition of the Perry's Chemical Engineering Handbook [3], empirical correlations for the total emissivities of water vapor, carbon dioxide, and four mixtures of the two gases are provided. Empirical constants are available at temperatures of 1000, 1500 and 2000 K and for H_2O/CO_2 partial pressure ratios of 0, 0.5, 1.0, 2.0, 3.0 and ∞. These correlations were developed based on the data in Hottel emissivity charts [15] and were adjusted using more

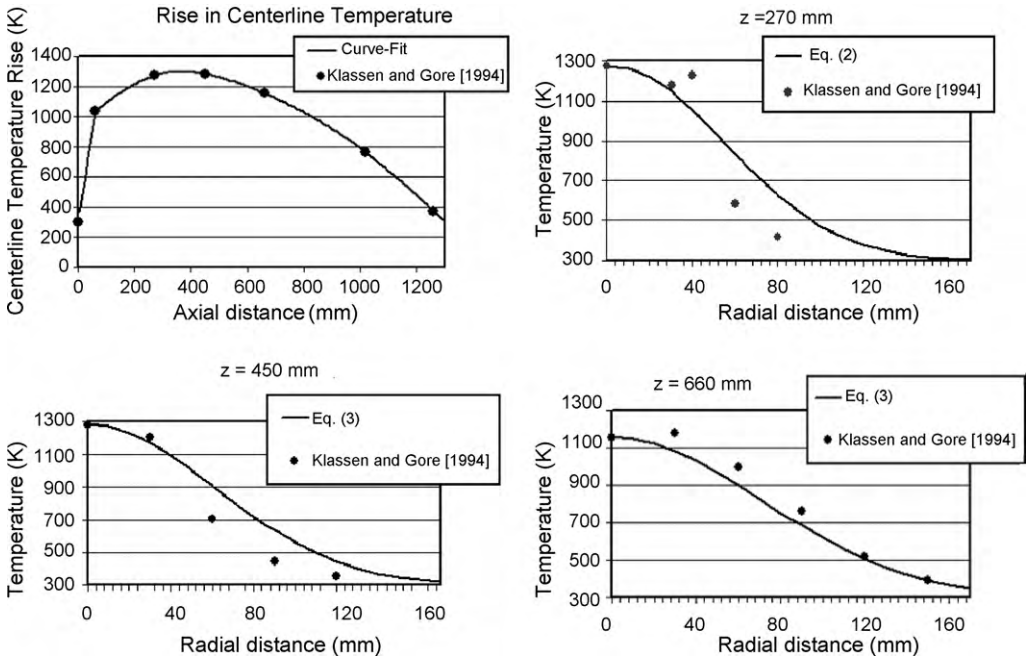

Fig. 2. The mean temperature profiles at various axial and radial locations in the 30 cm heptane pool fire.

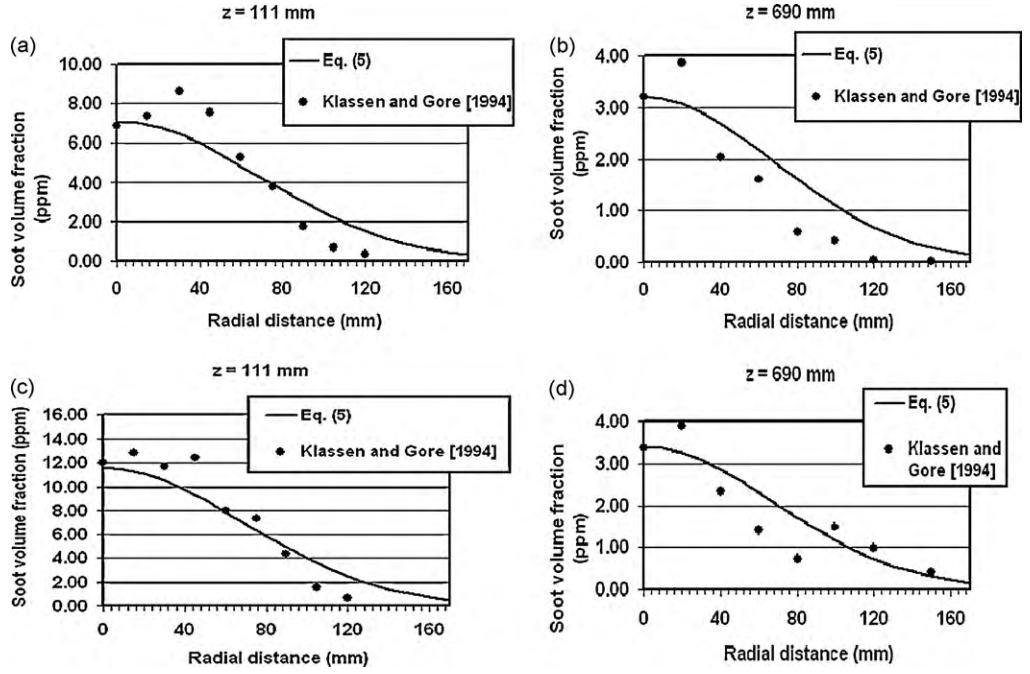

Fig. 3. The radial mean soot profiles at various axial locations in the 30 cm toluene pool fire: (a) and (b) emission soot; (c) and (d) absorption soot.

recent data from RADCAL [5]. For calculating emissivities at other temperatures, linear interpolation or extrapolation of the constants is recommended in the handbook [3]. The constants available at H_2O/CO_2 partial pressure ratios of 0.5 and 1.0 were employed to compute the total emissivities in this study. The empirical constants at these two ratios can be employed to compute gas emissivities for H_2O/CO_2 ratios ranging between 0.25–0.67 and 0.67–1.5 respectively. The results from this model are henceforth referred to in this work as "Perry."

A new WSGG model with four gray gases was recently developed based on a least-square fit to the total emissivities from the Perry model [16]. The WSGG model expresses the total gas emissivity as a weighted-sum-of-gray-gas emissivities:

$$\varepsilon = \sum_{j=0}^{3} a_j(T)\left[1 - \exp(-k_j L)\right] \tag{10}$$

In Eq. (10), a_j and κ_j are the emission weighting factor and the absorption coefficient for the jth gray gas component respectively, and L is the path length. The coefficients a_j and κ_j were obtained from a fit to total emissivity with the constraint that the sum of coefficients a_j is equal to unity. The transparent regions of the spectrum are accounted for by the term $j = 0$. The temperature dependence of

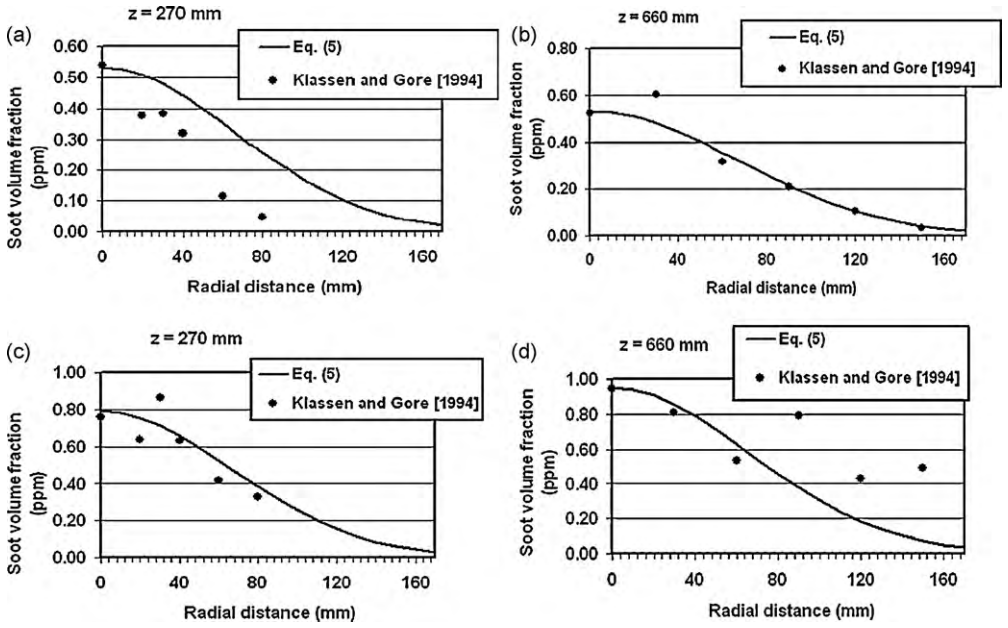

Fig. 4. The radial mean soot profiles at various axial locations in the 30 cm heptane pool fire: (a) and (b) emission soot; (c) and (d) absorption soot.

a_j is expressed as:

$$a_j(T) = C_1 T + C_2 \tag{11}$$

Details of the model are available in [16]. Four gray-gases were employed in this model to account for the non-gray behavior of gases and the model results are designated as "Perry (4 GG)" in this study.

3.3. Exponential wide band model (EWBM)

An exponential wide band model [4] based on a model first proposed by Edwards [17] was also employed in this study. The total gas band absorptance over a wide range of temperature, composition and path length conditions are described by three physical parameters: the integrated band intensity, the line-width-to-spacing parameter and the bandwidth parameter. Band averaged transmissivities are first computed from total gas band absorptance and an optical thickness. Total transmissivities are computed from the band averaged transmissivities by integrating over the spectrum using the 'block approximation' described in Lallemant and Weber [4]. The results from this model are designated as "EWBM." It is important to point out at this point that the coefficients in the Smith WSGGM [14] were obtained through curve-fits to the total emissivities from EWBM calculations. Therefore, although the Smith WSGGM [14] and the EWBM are based on the same spectroscopic or experimental database, this study will help examine the errors from employing the Smith WSGG coefficients developed for a H_2O/CO_2 ratio of 1 at H_2O/CO_2 ratios of 0.57 and 1.14 within the two fires.

3.4. Total emissivities from RADCAL

RADCAL [5] is a narrow band model that adopts the Curtis-Godson approximation together with the single line group (SLG) model [18] to compute the spectral intensities from a non-isothermal mixture of combustion gases and soot, incident upon a volume element. Details of this calculation procedure can be found in [5] and [18]. In this study, total emissivities were obtained from the spectral optical depth (X_η) computed by RADCAL at each narrow band and the mean beam length (L) of the geometry according to the equation:

$$\varepsilon_{\text{Total}} = \frac{\int I_{b\eta}(1 - e^{-X_\eta})\,\mathrm{d}\eta}{\int I_{b\eta}\,\mathrm{d}\eta} \tag{12}$$

The series summation proposed by Chang and Rhee [19] was used to determine the fractions of the black body functions ($I_{b\eta}$) corresponding to each spectral interval. The results from this model are designated as "RADCAL."

3.5. SLW

Non-gray calculations employing the spectral-line based weighted-sum-of-gray-gases model (SLW) proposed by Denison and Webb [20] was also employed in this study. In the SLW model, the absorption cross-section domains of H_2O and CO_2 were each discretized into 20 logarithmically spaced intervals between 3×10^{-5} and 120 $m^2\,mol^{-1}$ and 3×10^{-5} and 600 $m^2\,mol^{-1}$ respectively. The correlations presented in [21,22] for the absorption-line blackbody distribution functions (ALBDF) of H_2O and CO_2 were used to compute the blackbody weights. The multiplication approach to the calculation of the ALBDF was employed to compute the blackbody weights for the H_2O–CO_2 mixture [23]. The radiative transport equation was then solved for 21 gray gases employing this approach. The results from this model are designated as "SLW (21 GG)."

4. Radiative property of soot

The soot absorption coefficient was estimated as [24]:

$$k_s = \frac{3.72 f_v C_0 T}{C_2}, \quad \mathrm{m}^{-1} \tag{13}$$

where

$$C_0 = \frac{36\pi n\kappa}{\left(n^2 - \kappa^2 + 2\right)^2 + 4n^2\kappa^2}; \quad C_2 = 1.4388\,\mathrm{cm\,K};$$
$$n = 1.55; \quad \kappa = 0.56 \tag{14}$$

In Eq. (14), the optical constants n and κ are based on the measurements of Dalzell and Sarofim [10]. This is consistent with the

optical constants employed in the experiments to infer the soot volume fractions.

5. Discrete ordinates (DO) method

The radiation calculations in this study were carried out employing an in-house DO radiation code. If ζ_m, μ_m and η_m represent the direction cosines associated with each ordinate direction, k the absorption coefficient and I_b the black body emissive power, then the differential equation governing the DO method in the absence of scattering can be written for each direction "m" as [25]:

$$\zeta_m \frac{\partial I_m}{\partial x} + \mu_m \frac{\partial I_m}{\partial y} + \eta_m \frac{\partial I_m}{\partial z} = -kI_m + kI_b \tag{15}$$

When the presence of cold soot was included in the calculations, the cold soot temperature was set at 298 K and the radiative transport equation was expressed as:

$$\zeta_m \frac{\partial I_m}{\partial x} + \mu_m \frac{\partial I_m}{\partial y} + \eta_m \frac{\partial I_m}{\partial z} = -(k + k_{\text{cold soot}})I_m + kI_b + k_{\text{cold soot}} I_{b,\ \text{cold soot}} \tag{16}$$

The boundary condition associated with the above equation considering the surrounding surfaces to be black is:

$$I_m = I_b \tag{17}$$

The radiative heat fluxes within the domain or at a surface and the radiative flux divergence was determined as [25]:

$$\mathbf{q}(\mathbf{r}) = \int_{4\pi} I(\mathbf{r}, \hat{\mathbf{s}})\hat{\mathbf{s}}\, \mathrm{d}\Omega \approx \sum_m w_m I_m(\mathbf{r})\hat{\mathbf{s}}_m \tag{18}$$

$$\nabla \bullet \mathbf{q}(\mathbf{r}) = k(\mathbf{r})(4\pi I_b(\mathbf{r}) - G(\mathbf{r})) \tag{19}$$

When cold soot was taken into account, the radiative source term was computed as:

$$\nabla \bullet \mathbf{q}(\mathbf{r}) = k(\mathbf{r})(4\pi I_b(\mathbf{r}) - G(\mathbf{r})) + k_{\text{cold soot}}(4\pi I_{b,\ \text{cold soot}}(\mathbf{r}) - G(\mathbf{r})) \tag{20}$$

G, the incident radiation was calculated as:

$$G(\mathbf{r}) = \int_{4\pi} I(\mathbf{r}, \hat{\mathbf{s}})\, \mathrm{d}\Omega \approx \sum_m w_m I_m(\mathbf{r}) \tag{21}$$

In Eqs. (18) and (21), w_m is the angular weight associated with each direction "m". In this study, the T_4 angular quadrature scheme [26] was used in conjunction with the DO model. This solves the DO equation in 128 directions. Based on the conclusions of Jensen et al. [1] and Hostikka [2], this angular resolution was deemed to be adequate to accurately predict radiative fluxes within and away from the pool fire. A finite-volume discretization to Eqs. (15) and (16) was performed in this study. Multiplying both sides of Eqs. (15) and (16) by $\mathrm{d}V = \mathrm{d}x\,\mathrm{d}y\,\mathrm{d}z$, and integrating over the volume elements, the intensity I_m at the center of each control volume in a uniform, structured grid is related to the face centered values of the intensities as:

$$\zeta_m A\left[I_{m,i+1} - I_{m,i}\right] + \mu_m B\left[I_{m,j+1} - I_{m,j}\right] + \eta_m C\left[I_{m,k+1} - I_{m,k}\right] = -kI_m V + kI_b V \tag{22}$$

where A, B and C represent the surface areas of the faces of the volume element that are normal to the x-, y- and z-axes respectively, and i, j and k represent the surface element indices along the x-, y- and z-axes respectively. The upwind differencing scheme was employed to relate the face centered values to the cell centered values. For directions with positive direction cosines, this results in:

$$I_{m,i+1} = I_{m,j+1} = I_{m,k+1} = I_m \tag{23}$$

A similar analysis can be carried out for other combinations of direction cosines as well. Substituting Eq. (23) in Eq. (22) we get:

$$[\zeta_m A + \mu_m B + \eta_m C + kV]\, I_m = \zeta_m A I_{m,i} + \mu_m B I_{m,j} + \eta_m C I_{m,k} + kI_b V \tag{24}$$

Thus, Eq. (24) corresponds to a discretized set of linear algebraic equations of the form:

$$P_p I_{m,p} + \sum_s P_s I_{m,s} = Q_p \tag{25}$$

where, the subscript p corresponds to the node at which Eq. (15) is being approximated, the index "s" runs over all the neighboring surface nodes in Eq. (22), P_s corresponds to the product of the direction cosines with the geometric properties (surface areas) and Q_p contains all the terms that are known. Eq. (25) can be written is matrix form as:

$$PI_m = Q \tag{26}$$

where, "P" corresponds to a square coefficient matrix. In this study, a Gauss-Siedel iterative scheme was employed to solve the matrix equations.

6. Turbulence–radiation interactions (TRI)

In combustion systems, the local turbulent fluid mechanics influences the radiation field through fluctuations in temperature and species concentrations, which in turn influence the absorption coefficients (k) and the emission source term (kI_b). Various approaches to model TRI have been reviewed by Coelho [27]. However, based on data from heavily sooting acetylene-air flames, Gore and Faeth [28] suggested that TRI effects in heavily sooting flames are dominated by the temperature self-correlation effect. The essence of computing the temperature self-correlation in TRI models reduces to the calculation of $\overline{T^4}$ in the emissive power term (I_b) in the time-averaged radiative transfer equation (RTE). Burns [29] showed that $\overline{T^4}$ can be approximated from mean and standard deviation of temperature by expanding the Planck's black body emissive power in a Taylor series about the mean temperature and time averaging [29]:

$$\frac{\overline{T^4}}{\overline{T}^4} = \left(1 + 6\frac{\overline{T'^2}}{\overline{T}^2} + 4\frac{\overline{T'^3}}{\overline{T}^3} + \frac{\overline{T'^4}}{\overline{T}^4}\right) \tag{27}$$

While carrying out simulations of propane pool fires, for temperature fluctuation intensities ($\sqrt{\overline{T'^2}}/\overline{T}$) less than 0.6, Snegirev [6] approximated this as:

$$\frac{\overline{T^4}}{\overline{T}^4} \approx \left(1 + 5.5\frac{\overline{T'^2}}{\overline{T}^2}\right) \tag{28}$$

Eq. (28) was employed in this study to estimate the time-averaged emissive power for computing I_b in Eqs. (15), (16) and (20).

7. Results and discussion

The decoupled radiative transfer calculations for this fire were carried out in a domain of size 0.91 m × 0.91 m × 1.30 m, with the longest dimension being along the vertical axis. A uniform grid size

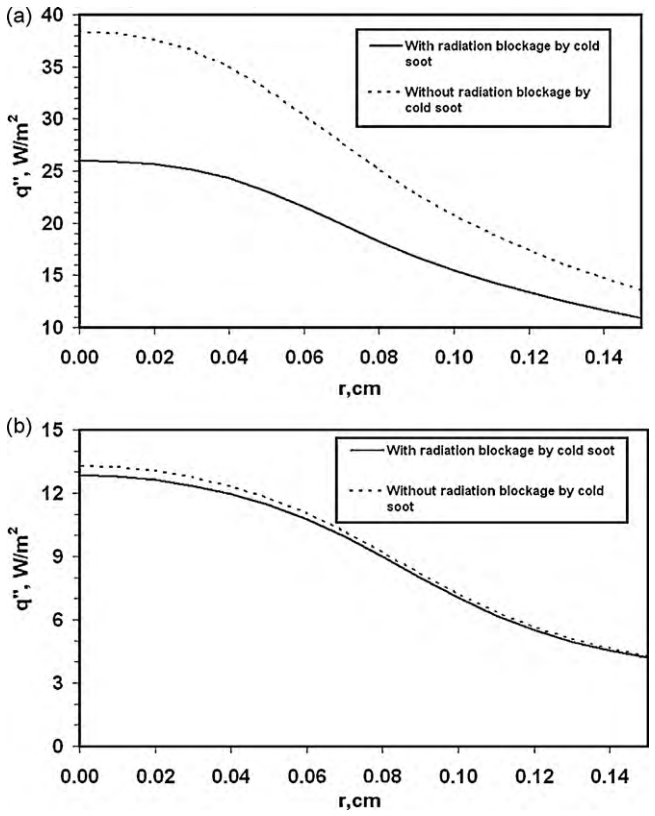

Fig. 5. The effect of radiation blockage on the radiative fluxes to the pool surface: (a) toluene pool fire; (b) heptane pool fire.

of 1 cm × 1 cm × 1 cm was employed in the calculations to match the spatial resolution of the experimental measurements. Fig. 5 shows the effect of cold soot on the radiative fluxes to the pool surface. The calculations were performed employing the Perry (4 GG) model. In the heavily sooting toluene pool fire, the presence of cold soot particles near the pool surface absorb and block the radiation, thereby suppressing the radiative feedback to the pool surface. The average radiation feedback to the pool surface is reduced by 27% in the toluene fire and by less than 3% in the moderately sooting heptane fire. Since the radiative feedback strongly influences the rates of fuel pyrolysis and vaporization, the need to model the cold soot volume fraction is critical in CFD simulations particularly when a fuel pyrolysis sub-model is employed in conjunction with the combustion models. Therefore, unless stated otherwise all the subsequent results in this study include the effects of cold soot particles. Fig. 6(a) and (b) show the fractional contributions to the radiant heat flux at the pool surface from the emission soot at different axial locations. The effects of gas absorption and cold soot are not included here. The results are seen to agree well with the corresponding emission soot calculations of Klassen and Gore [9]. The results also show that in the toluene pool fire, most of the radiation feedback occurs within the axial location $x/D < 1$. Radiation from $x/D > 1$ does not reach the pool surface due to soot self-absorption. In the case of heptane pool fire however, soot radiation from higher axial locations also reach the pool surface. Any differences in Figs. 6 between the numerical predictions of Klassen and Gore [9] and this study may be attributed to the following. Klassen and Gore [9] performed the radiation analysis based on transient measurements of temperature and soot volume fractions in conjunction with a simplified treatment of turbulence–radiation interactions to estimate directional and hemispherical radiative heat feedback to the fuel surface. The 1D line of sight radiation calculations in their study approximately accounted for the variations in the soot transmissivities as well as the emissive power terms due to turbulent fluctuations. The 3D radiation calculations in this study although accounts for the time-averaged emissive power [cf. Eq. (28)], employs mean soot volume fractions to compute the radiative properties. Furthermore, the use of correlations [cf. Eqs. (1)–(5)] to generate the temperature and soot concentration fields in this study might also contribute to the resulting differences. In order to rigorously account for the fluctuations in the absorption coefficient in the radiation calculations would require simultaneous single shot measurements of soot concentrations and temperature at different spatial locations to compute an appropriate time-averaged absorption coefficient. Fig. 7 shows the axial and radial radiative flux predictions employing different gray and non-gray models. In both the pool fires, the variations among the gray and the non-gray models due to differences in the spectroscopic databases employed in the model formulation are seen to be small (<10%). In the toluene pool fire, where the radiation is dominated by the gray soot, the differences between the gray and non-gray modeling strategies are also small. However, in case of the heptane pool fire, there is a clear grouping and distinction between the gray and non-gray model results. In Fig. 7, the results from the Perry (4 GG) and Smith (4 GG) models are seen to be very close to those obtained from the SLW model although these models were run at only a fraction of the computational cost of the SLW model (4 bands versus 21 in the SLW model). Optimization of the SLW model coefficients may be carried out to decrease this difference in computational time. However, this was not undertaken in this study. Fig. 8 shows the centerline variation in the radiative source term predictions employing different gray and non-gray models. In case of the toluene pool fire, since the gray soot radiation is the dominant contributor to the radiative source term, there is little variation among the model predictions. For the heptane pool fire however, the maximum average variation was found to be 13% among the non-gray models and 21% among the gray models. If about 30% of the total heat released in pool fires were to be associated with radiation, then a 20% variation in the radiative source terms among the property models would result in a temperature difference of about 6% in a fully coupled calculation. At a peak temperature of 1500 K, this would correspond to a difference of 90 K caused by differences due to the property model

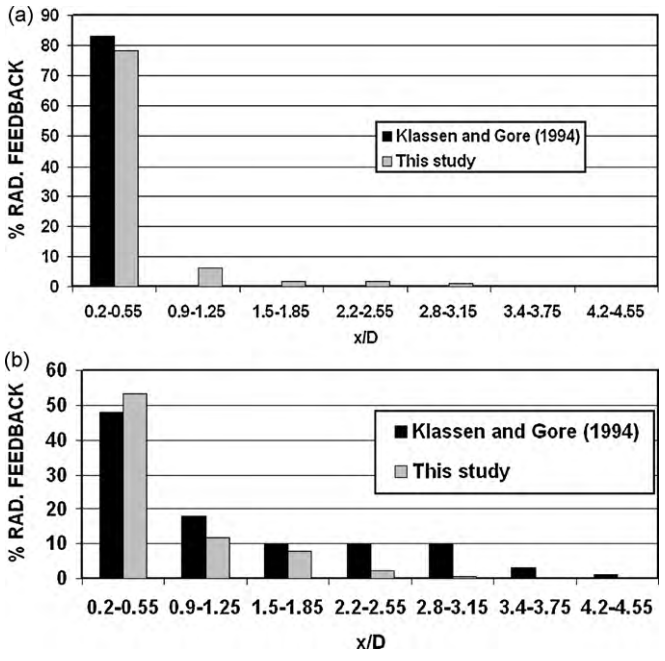

Fig. 6. The fraction of radiative feedback to the pool surface from emission soot at different axial locations: (a) toluene pool fire; (b) heptane pool fire.

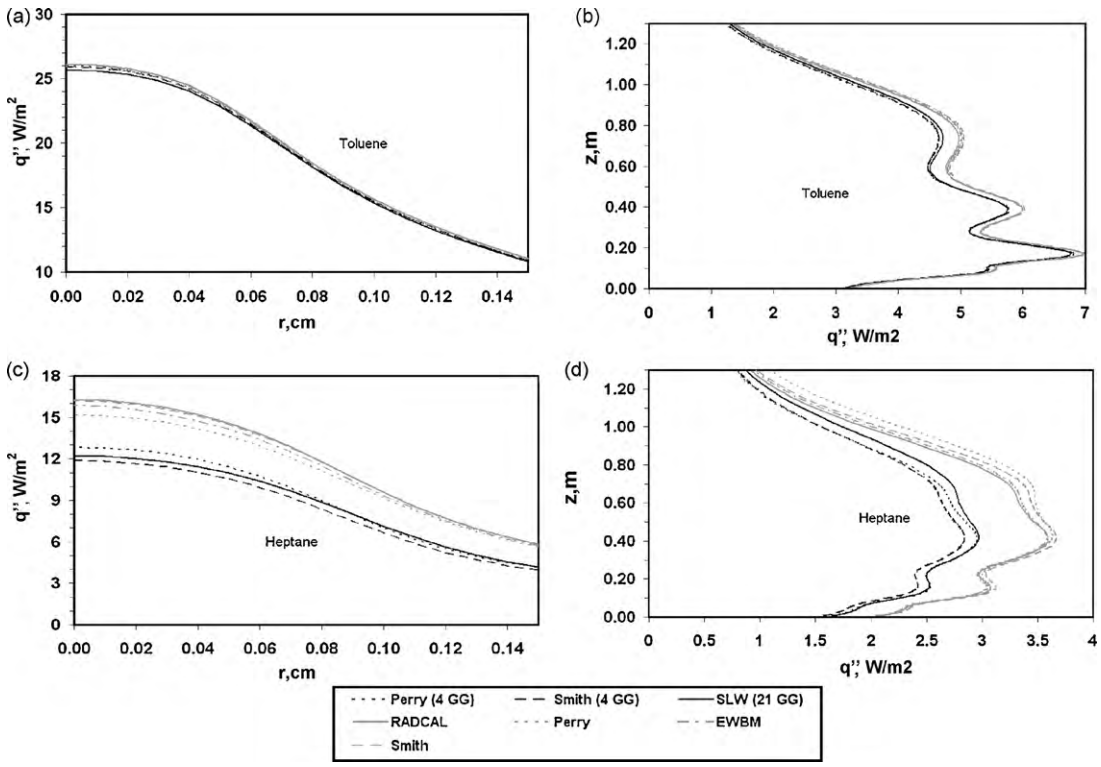

Fig. 7. Radiative flux predictions employing different gray and non-gray radiative property models: (a) and (c) radial radiative fluxes to the pool surface; (b) and (d) axial radiative fluxes at a distance of 45.5 cm from the pool center.

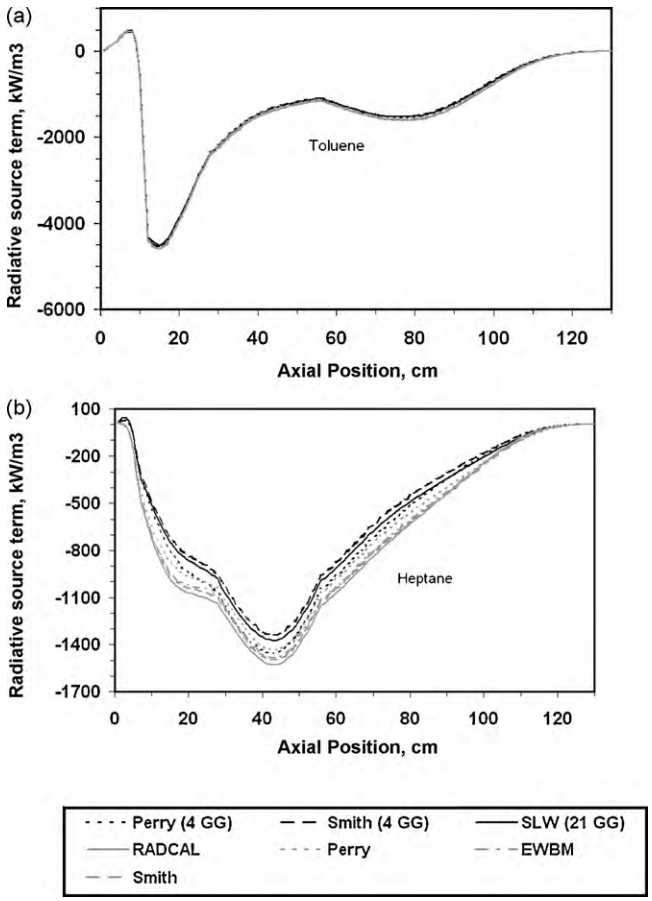

Fig. 8. Centerline radiative source term predictions employing different gray and non-gray radiative property models: (a) Toluene pool fire; (b) Heptane pool fire.

spectroscopic databases. Although the variation is observed to be smaller in highly sooting fires such as toluene, in moderately sooting fires where gas radiation is also important, these differences can influence soot formation and flame extinction. The axial and radial radiative flux predictions due to gas radiation in the heptane and toluene pool fires are shown in Fig. 9. Similar to the radiative source term predictions, the differences in the spectroscopic databases cause a 10–20% variation in the gas radiative heat fluxes. The extent of this variation is in line with the study of Lallemant et al. [30] where a 20% variation in the total gas emissivities predicted by various models was reported. Furthermore, there is a clear grouping and distinction between the gray and non-gray results in Fig. 9. The gray model fluxes are seen to be about 40–50% higher than the non-gray fluxes when the path length employed to predict the radiative properties is obtained from Eq. (9). In order to improve the agreement between the gray and non-gray formulations, a corrected mean beam length of 0.3 × geometric mean beam length in the Perry model was employed next to compute the gas emissivities and the absorption coefficients. Fig. 10 compares the axial and radial radiative fluxes due to gas radiation predicted by employing this corrected path length in the Perry model against the non-gray models. The corrected mean beam length is seen to improve the agreement in the heat flux predictions between the gray and non-gray models. When simulating open pool fires or fires in a crosswind, the fire geometry can take different shapes and sizes and occupy only a fraction of the overall computational domain. In such scenarios, the path length that is to be employed to determine the gas-phase radiative properties cannot be determined in a straight forward manner. Analogous to the procedure employed in this study, path length independent non-gray calculations can be performed on an approximate steady state fire shape and the path length in the gray model can be adjusted to match the non-gray model results. Benchmark non-gray data for use in this procedure may be generated through the SLW model or the more rigorous full-spectrum K-distribution method that has

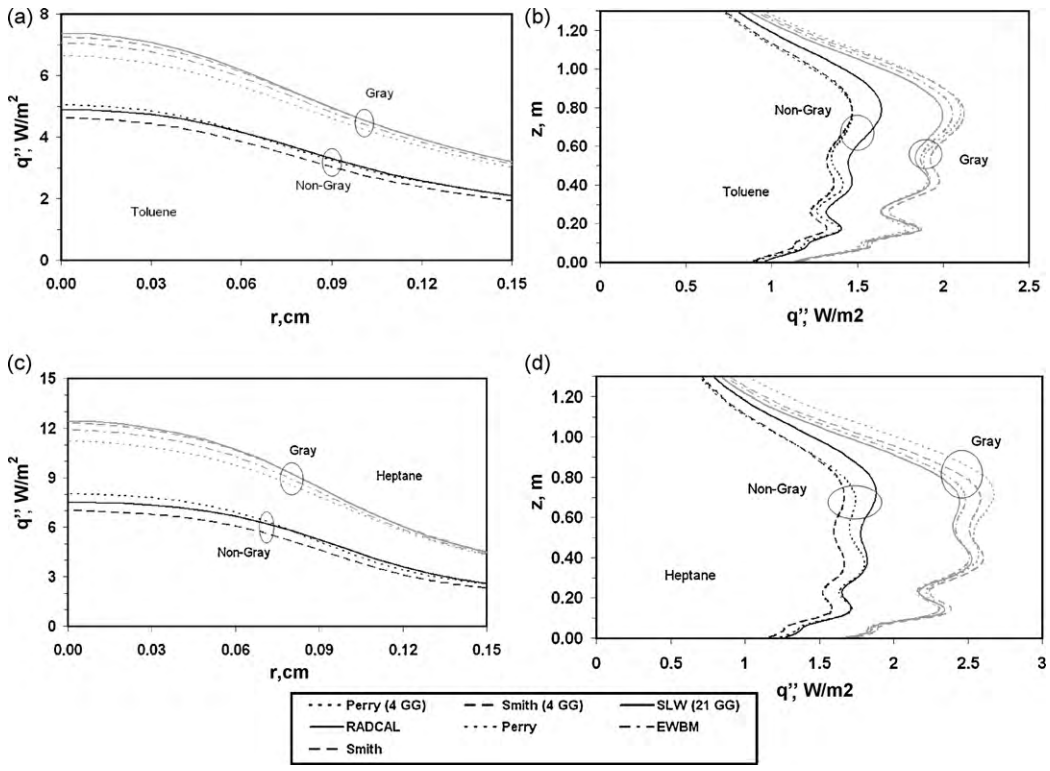

Fig. 9. Radiative flux predictions (gas radiation only) employing different gray and non-gray radiative property models: (a), (c) Radial radiative fluxes to the pool surface; (b), (d) Axial radiative fluxes at a distance of 45.5 cm from the pool center.

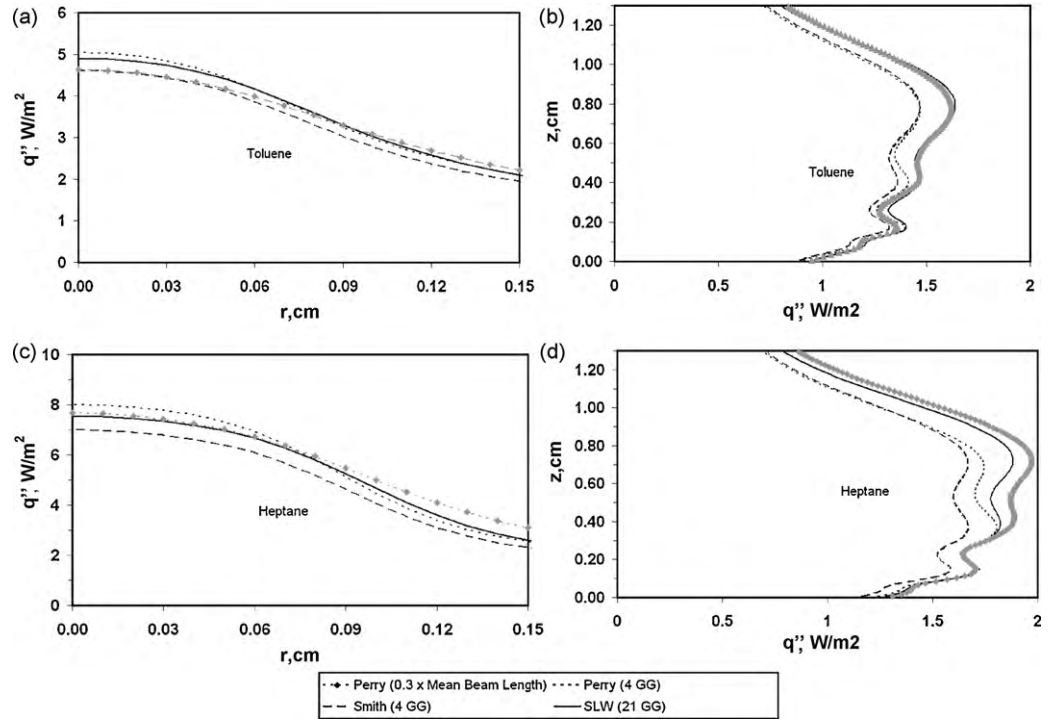

Fig. 10. Radiative flux predictions (gas radiation only) employing different non-gray models and the Perry model employing a corrected mean beam length: (a) and (c) radial radiative fluxes to the pool surface; (b) and (d) axial radiative fluxes at a distance of 45.5 cm from the pool center.

been developed and improved by Modest and his colleagues in recent years [31–33]. These models have been developed from and validated against highly accurate line-by-line spectroscopic data. The path length corrected gray model can then be employed through the rest of the transient simulation to avail savings in computational time. Although the cases examined in this study were limited to medium scale pool fires, total emissivity correlations such as the Smith model have been relatively successful in predicting radiative transfer during coal combustion in full scale utility boilers where the mean beam length of the geometry is

well defined and the domain geometry and radiative power output are much larger [16]. Therefore, it can be anticipated that a mean beam length for gas radiation appropriately computed based on the methodology described above may be employed to improve the agreement between gray and non-gray modeling in pool fires of various sizes and shapes. However, it can be recognized that radiation in large-scale pool fires are often dominated by soot (whose radiative properties may be considered to be mean-beam length independent, cf. Eq. (13)) that can mask the importance of gas radiation thereby alleviating the need to come up with a very accurate mean beam length for the gas radiative properties. In the wide and narrow band models employed in this study (EWBM and RADCAL), several mathematical operations involving various band parameters were performed to compute band averaged properties within each band and these were integrated across the entire spectrum to compute a total property. These incurred a significant computational overhead in the calculations since these operations had to be performed at each computational cell. Although pre-computing and tabulating these absorption coefficients as a function of CO_2, H_2O and temperature can provide computational savings [2], these tables would need to be generated for every new geometry due to its dependence on the domain mean beam length. Comparisons of the Smith and the EWBM model results in Figs. 7–10 show that the errors due to the use of the Smith WSGG [14] model coefficients developed for H_2O/CO_2 ratios of 1 at H_2O/CO_2 ratios of 0.57 and 1.14 are small. Since the emissivity calculations of the Smith model are computationally faster than the EWBM calculations, total emissivity correlations such as the Smith model and the Perry model with a corrected mean beam length may be employed in large-scale, transient, simulations of pool fires.

8. Conclusions

Decoupled radiative heat transfer calculations of 30 cm-diameter toluene and heptane pool fires were performed employing the discrete ordinates method. Detailed experimental measurements of soot volume fractions based on absorption and emission, temperature statistics in conjunction with correlations found in the literature were employed to create the composition and temperature fields within the fires. The interaction between turbulence and radiation was accounted for through the temperature self-correlation term which was estimated based on the measured temperature variance data. The performances of four gray and three non-gray gas radiative property models were compared. Based on the results of this study, the following conclusions can be drawn:

1. By employing the measured absorption and emission soot volume fractions, the effects of radiation blockage due to the presence of cold soot near the fuel surface were examined. In the heavily sooting toluene pool fire, the presence of cold soot particles suppressed the average radiation feedback to the pool surface by about 27% whereas in the case of the moderately sooting heptane pool fire, the corresponding difference was less than 3%.
2. The average variation in the radiative transfer predictions among the property models due to differences in the spectroscopic databases employed in the model formulations was between 10% and 20%.
3. Clear differences were seen between the gray and non-gray model results when the mean beam length was computed based on traditionally employed geometric relations. Therefore, a correction to the mean beam length was suggested to improve the agreement between gray and non-gray modeling in simulations of open pool fires.
4. A comparison of the Smith WSGG and the EWBM model results showed that the errors due to the use of the Smith WSGG model coefficients developed for H_2O/CO_2 ratios of 1 at H_2O/CO_2 ratios of 0.57 and 1.14 were small. Although the cases examined in this study were limited to medium scale pool fires, recent simulations of coal combustion in a full scale utility boiler (where the domain geometry and radiative power output are much greater) have also revealed that the gas-phase absorption coefficients predicted employing total emissivity correlations in the Smith and Perry model are close to those predicted employing the EWBM [16]. Since the Smith and Perry models are computationally faster than the EWBM, the total emissivity correlations in these models with a corrected mean beam length can therefore potentially be employed in large-scale, transient, simulations of pool fires.
5. The fraction of radiative feedback to the pool surfaces from emission soot at different axial locations agreed well with the results from the experimental study. Therefore, comprehensive, 3D, decoupled radiation calculations performed in this study through interpolations and extrapolations of detailed experimental measurements have enabled us to develop a CFD validation methodology to examine pool fires of various sooting propensities.

References

[1] K.A. Jensen, J.F. Ripoll, A.A. Wray, D. Joseph, M.E. Hafi, On various modeling approaches to radiative heat transfer in pool fires, Combust. Flame 148 (2007) 263–279.
[2] S. Hostikka, Development of fire simulation models for radiative heat transfer and probabilistic risk assessment, Thesis, Helsinki University of Technology, VTT Technical Research Centre of Finland, 2008.
[3] H.C. Hottel, J.J. Noble, A.F. Sarofim, Heat and mass transfer, in: D.W. Green, R.H. Perry (Eds.), Perry's Chemical Engineers' Handbook, 8th ed., McGraw-Hill, New York, 2007 (Chapter 5).
[4] N. Lallemant, R. Weber, A computationally efficient procedure for calculating gas radiative properties using the exponential wide band model, Int. J. Heat Mass Transf. 39 (1996) 3273–3286.
[5] W.L. Grosshandler, RADCAL: a narrow-band model for radiation calculations in a combustion environment, NIST Technical Note 1402, 1993.
[6] A.Yu. Snegirev, Statistical modeling of thermal radiation transfer in buoyant turbulent diffusion flames, Combust. Flame 136 (2004) 51–71.
[7] P.J. Coelho, O.J. Teerling, D. Roekaerts, Spectral radiative effects and turbulence/radiation interaction in a non-luminous turbulent jet diffusion flame, Combust. Flame 133 (2003) 75–91.
[8] P.J. Coelho, Detailed numerical simulation of radiative transfer in a nonluminous turbulent jet diffusion flame, Combust. Flame 136 (2004) 481–492.
[9] M. Klassen, J.P. Gore, Structure and radiation properties of pool fires, NIST-GCR-94-651, 1994.
[10] W.H. Dalzell, A.F. Sarofim, Optical constants of soot and their application to heat-flux calculations, J. Heat Transf. 91 (1969) 100–104.
[11] B.J. McCaffrey, Momentum implications for Buoyant diffusion flames, Combust. Flame 52 (1983) 149–167.
[12] X.L. Zhang, J.P. Vantelon, P. Joulain, A.C. Fernandez-Pello, Influence of an external radiant flux on a 15-cm-diameter kerosene pool fire, Combust. Flame 86 (1991) 237–248.
[13] A. Shinotake, S. Koda, K. Akita, An Experimental study of radiative properties of pool fires of an intermediate scale, Combust. Sci. Technol. 43 (1985) 85–97.
[14] T.F. Smith, Z.F. Shen, J.N. Friedman, Evaluation of coefficients for the weighted sum of gray gases model, Int. J. Heat Mass Transf. 47 (2004) 1367–1382.
[15] H.C. Hottel, A.F. Sarofim, Radiative Transfer, 1st ed., McGraw-Hill, New York, 1967.
[16] G. Krishnamoorthy, S.A.L. Perera, S. Orsino, M. Shahnam, D.E. Huckaby, Radiation modelling in oxy-fuel combustion scenarios, Int. J. Comput. Fluid Dyn. in press.
[17] D.K. Edwards, Molecular gas band radiation, Adv. Heat Transf. 12 (1976) 115–193.
[18] C.B. Ludwig, W. Malkmus, J.E. Reardon, J.A.L. Thomson, Handbook of infrared radiation, NASA SP-3080, Washington, DC, 1973.
[19] S.L. Chang, K.T. Rhee, Blackbody radiation functions, Int. Commun. Heat Mass 11 (1984) 451–455.
[20] M.K. Denison, B.W. Webb, A Spectral line-based weighted-sum-of-gray-gases model for arbitrary RTE solvers, ASME J. Heat Transf. 115 (1993) 1004–1012.
[21] M.K. Denison, B.W. Webb, An absorption-line blackbody distribution function for efficient calculation of total gas radiative transfer, J. Quant. Spectrosc. Radiat. 50 (1993) 499–510.

[22] M.K. Denison, B.W. Webb, Development, Application of an absorption-line blackbody distribution function for CO_2, Int. J. Heat Mass Transf. 38 (1995) 1813–1821.
[23] V.P. Solovjov, B.W. Webb, SLW modeling of radiative transfer in multicomponent gas mixtures, J. Quant. Spectrosc. Radiat. 65 (2000) 655–672.
[24] M.J. Yu, S.W. Baek, J.H. Park, An extension of the weighted sum of gray gases non-gray radiation model to a two phase mixture of non-gray gas with particles, Int. J. Heat Mass Transf. 43 (2000) 1699–1713.
[25] M.F. Modest, Radiative Heat Transfer, 2nd ed., Academic Press, New York, 2003.
[26] C.P. Thurgood, A. Pollard, A.B. Becker, The T_N quadrature set for the discrete ordinates method, ASME J. Heat Transf. 117 (1995) 1068–1070.
[27] P.J. Coelho, Numerical simulation of the interaction between turbulence and radiation in reactive flows, Prog. Energy Combust. 33 (2007) 311–383.
[28] J.P. Gore, G.M. Faeth, Structure and radiation properties of luminous turbulent acetylene/air diffusion flames, ASME J. Heat Transf. 110 (1988) 173–181.
[29] S.P. Burns, Turbulence radiation interaction modeling in hydrocarbon pool fire simulations, Sandia Report, SAND99-3190, Sandia, New Mexico, 1999.
[30] N. Lallemant, A. Sayre, R. Weber, Evaluation of emissivity correlations for H_2O–CO_2–N_2/air mixture and coupling with solution methods of the radiative transfer equation, Prog. Energy Combust. 22 (1996) 543–574.
[31] M.F. Modest, Narrow-band and full-spectrum k-distribution for radiative heat transfer correlated-k vs. scaling approximation, J. Quant. Spectrosc. Radiat. 76 (2003) 69–83.
[32] M.F. Modest, H. Zhang, The full-spectrum correlated-k distribution for thermal radiation from molecular gas particulate mixtures, ASME J. Heat Transf. 124 (2002) 30–38.
[33] M.F. Modest, R.J. Riazzi, Assembly of full-spectrum k-distributions from a narrow-band database; effects of mixing gases, gases and nongray absorbing particles, and mixtures with nongray scatters in nongray enclosures, J. Quant. Spectrosc. Radiat. 90 (2005) 169–189.